Extremal Hawking radiation

Michael R. R. Good

Physics Department & Energetic Cosmos Laboratory, Nazarbayev University, Nur-Sultan, Kazakhstan

(Received 19 March 2020; accepted 11 May 2020; published 26 May 2020)

The particle spectrum for collapse to an extremal Reissner-Nordström black hole is solved by use of the corresponding moving mirror model. The amount of particles and energy flux is symmetric in delayed null time as received by an observer at infinity. The star emits a total finite amount of energy carried by particles that are not specified by a temperature. The finite energy limits the evaporation process yet an infinite amount of particles with zero frequency characterize the radiation. At ultralate times the particle emission spectrum is that of a uniformly accelerated mirror.

DOI: 10.1103/PhysRevD.101.104050

I. INTRODUCTION

The extremal Reissner-Nordström (ERN) black hole has played an important and fascinating role in fundamental theoretical physics. It is the only static spherically symmetric black hole solution (electrovacuum) to Einstein's equations with zero surface gravity (i.e., undefined temperature [1,2]), and has been central to our nascent understanding of the *classical* thermodynamics of black holes. Furthermore, since extremal black holes have been crucial for development of a statistical origin of black hole entropy [3], their study has been fruitful for an understanding of the *quantum* statistical mechanics of black holes.

On the experimental side, there is the dynamical Casimir effect which has empirical confirmation (see [4] for a brief timely review and numerous references therein), promoting the 50 year old moving mirror model [5], to a laboratory demonstration of spontaneous emission of particles generated by an accelerated boundary condition. While the single moving mirror model [6–8] has a long history as an analog system for understanding late-time Hawking radiation [9], it continues to provide new insights into the equivalence principle's impact on the emission of particles in quantum theory [10,11] and the related Unruh effect [12].

The equivalence principle links both the collapse to an ERN black hole and an asymptotically uniformly accelerating moving mirror [1] because the main property of the incipient ERN is its zero surface gravity.

An observer moving along with the uniformly accelerated mirror will feel constant proper acceleration. This is similar to the force of gravity upwards felt by a standing observer on the Earth. Vice versa, by the equivalence principle, the curved spacetime of the ERN black hole results in zero acceleration of a static observer near the horizon as measured at infinity.

A. Early times vs late times

The equivalence principle links the two systems but this happens asymptotically at late times when the black hole is old. Our question is: *what happens at early times?* This is where the literal information content concerning collapse, as contained in the "extremal" radiation, is located. Twenty years ago Liberati-Rothman-Sonego (LRS) found the late-time behavior [1,13] of the spectrum of the ERN black hole. That is, they were the first to see that an incipient extremal black hole is modeled at late times by a uniformly accelerated mirror. Our results provide a focus on the early times by solving for the full all-time spectrum.

More specifically, the beta coefficients found by LRS are those of the uniformly accelerated mirror (e.g., [8,14]), and thus, only reveal that soft particles are created at some time in the late stages of collapse, which does not necessarily mean that particles carrying energy are emitted at late times. In fact, the results of LRS demand there is no energy radiated at late times. The soft particle production by itself does not contain the energy or information relevant to details of collapse, nor does it mean that particle creation takes place at a steady rate. We shall demonstrate the creation rate of all particles at all times, extracting information about the collapse. We do this by time evolving the particle creation with wave packet localization.

B. No-hair theorem and cosmic censorship conjecture

The spectra resulting from the $1+1$ dimensional mirror's worldline is the same as that of the ERN black hole, up to gray-body factors due to the unique ds^2 of ERN spacetime and due to the extra space dimensions of $3+1$ geometry. LRS concluded that incipient extremal RN black holes create particles with a nonthermal spectrum, and we demonstrate that the full nonasymptotic solution does indeed possess a nonthermal spectrum[1] for the ERN black hole, even during early collapse. With an exact analytic form of the global beta coefficients, the spectrum for all times, both past and future, reveals the particle production

[1]The thermal spectrum (eternal) is that from the trajectory of Carlitz-Willey [15,16].

evolution leading to the damping at late stages of collapse, concluding that the no-hair theorem is preserved because there is no way to extract information from infinite soft particles at late times.

One should suspect the cosmic censorship conjecture (CCC) to be violated because neutral scalar particles evaporating leads to a lessening of mass, M, all the while the star maintains a fixed charged Q, eventually leading to a flippening where the overbalance $Q^2 > M^2$ results in a naked singularity. However, we shall see that asymptotically the energy flux is zero, and only a finite amount of energy is evaporated, so that an old ERN black hole does not lose any more mass, despite the emission of particles. The CCC is actually preserved by the quantized fields [17], even though infinite particles (soft) are radiated. The results answer the question of how, in the presence of quantum radiation, the formation of a naked singularity is prevented.

This paper is organized as follows: Section II contains the ERN metric and matching condition for collapse. Section III constructs a moving mirror trajectory that models the null shell collapse to an ERN black hole, interpolating between vanishing velocity at early times and constant acceleration at late times. In Sec. IV we compute the stress tensor and total evaporation energy. Section V demonstrates both the time-localized and time-nonlocalized spectrum, particle count, a symmetry in time, and compares with the eternally uniform accelerated mirror. In Sec. VI we discuss limitations and extensions of the model, and in Sec. VII, we conclude. Units are $G = \hbar = c = 1$.

II. EXTREMAL REISSNER-NORDSTRÖM

The outside metric of the ERN collapse system, see Fig. 1, is given by the ERN geometry,

$$ds^2 = -\left(1 - \frac{M}{r}\right)^2 dt^2 + \left(1 - \frac{M}{r}\right)^{-2} dr^2 + r^2 d\Omega^2, \tag{1}$$

which is most simply interpreted as the exterior field of a spherically charged dust cloud in equilibrium between gravitational attraction and electrostatic repulsion [18]. Using the double null coordinate system (u, v), and $u = t - r^*$, and $v = t + r^*$, with the appropriate tortoise coordinate [19],

$$r^* = r + 2M \ln \frac{|r - M|}{M} - \frac{M^2}{r - M}, \tag{2}$$

one has the metric for the outside collapse geometry,

$$ds^2 = -f(r) du dv + r^2 d\Omega^2, \tag{3}$$

where

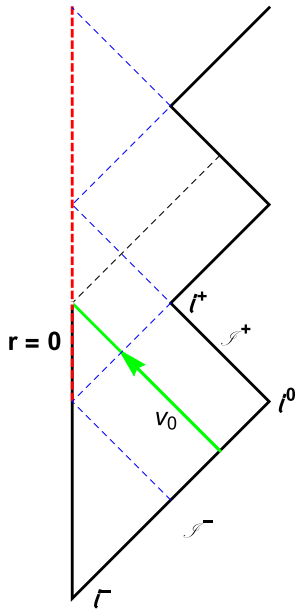

FIG. 1. A Penrose conformal diagram of a collapse of a null shell to form an extremal Reissner-Nordström black hole. The red dashed line is the irremovable timelike singularity. The black-red-dashed line is the position at $r = 0$ where modes pass through $r = 0$ but get lost nevertheless, never reaching $\mathscr{I}^+$. The thin dashed black line marks the last null ray that passes through $r = 0$ without hitting the singularity. The green line is the null shell, v_0. See Balbinot *et al.* [20], Fabbri-Navarro-Salas [19] and Carter [18] for illustrative ERN diagrams.

$$f(r) = \left(1 - \frac{M}{r}\right)^2. \tag{4}$$

As can be seen, the horizon is at $r = M$, and near it, spacetime looks like an infinite throat, see Fig. 2. The surface gravity is calculated to be $f'(r)|_{r=M} = 0$. Perhaps then, with this special "equilibrium," one would be led to think there is a temperature and that collapse may evolve to absolute zero, but what then is the spectrum of radiation during collapse? As is known, thermodynamics is not at play here (or at least categorically different), and we will show explicitly, the all-time spectrum is not Planckian. Even though the system temperature is left undefined, it is possible to find the nonthermal extremal Hawking radiation spectra.

The matching condition (see e.g., [1,19–21]) between the flat inside geometry, described by inside coordinates, $U = T - r$, and $V = T + r$, is the trajectory of the incipient black hole origin, expressed in terms of the outside function, $u(U)$, dependent on inside coordinate, U:

$$u(U) = U + \frac{4M^2}{(v_H - U)} - 4M \ln\left(\frac{v_H - U}{2M}\right). \tag{5}$$

The matching happens along the shell, v_0, where $v_0 - v_H \equiv 2M$. Regularity of the field at $r = 0$ ensures

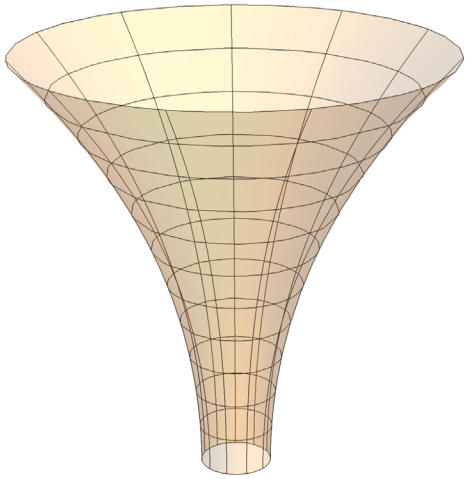

FIG. 2. Infinite throat, $r \to M$, with an asymptotically flat region for the spatial geometry of the ERN metric, Eq. (1). Setting $r = M(1+\epsilon)$, where ϵ is small, $ds^2 \approx -\epsilon^2 dt^2 + (M^2/\epsilon^2)d\epsilon^2 + M^2 d\Omega^2$. The first two terms are AdS_2, the last term is S^2. The spacelike distance between an outside point and $r = M$ horizon is infinite as computed by the proper length, $L = \int f^{-1/2} dr$. Timelike curves (and null rays) reach the horizon crossing the throat in a finite affine time. Evaluated at the horizon, Eq. (1) has zero surface gravity: "float in the throat."

the form of field modes, such that $U \leftrightarrow v$ identification can be made for the redshifting right movers. The mirror trajectory, $f(v) \leftrightarrow u(U)$, is then known, which we examine in the next section in the more simple background of flat space.[2]

III. TRAJECTORY AND DYNAMICS

For a massless scalar field in $1+1$ flat spacetime, the corresponding ERN moving mirror trajectory, where $\kappa \equiv 1/(2M)$, and $\kappa(v_0 - v_H) \equiv 1$, is

$$f(v) = v + \frac{1}{\kappa^2(v_H - v)} - \frac{2}{\kappa}\ln\left(\kappa(v_H - v)\right), \tag{6}$$

expressed in null coordinates (u, v) with u-function, $f(v)$, as a function of null coordinate advanced time v. The inverse is the usual advanced time v-function, $p(u)$, which is a function of retarded time u. Perhaps more intuitively, we express this motion in spacetime coordinates as a time, $t(x)$, function of coordinate space, x,

$$t(x) = v_H - \frac{1}{2\kappa W\left(\frac{e^{-\kappa x}}{2}\right)} - x. \tag{7}$$

[2]The geometry is not technically Minkowski because of the presence of the mirror.

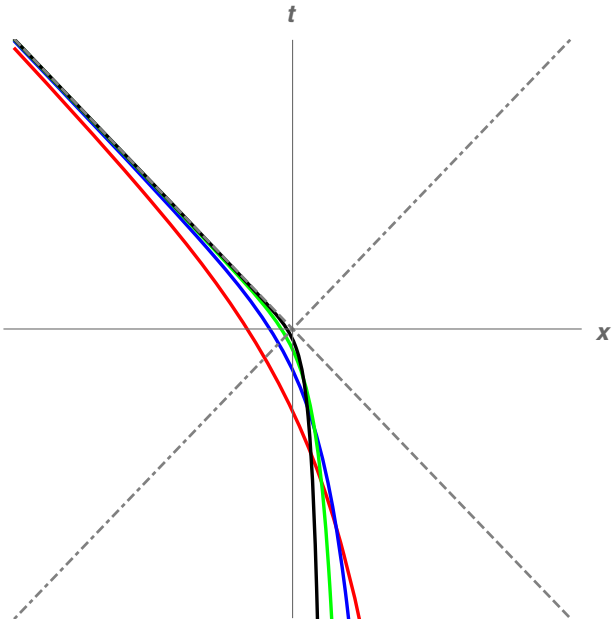

FIG. 3. The trajectory Eq. (7), in a spacetime plot, with different scaling for asymptotic future proper acceleration, κ. The red, blue, green, black curves correspond to $\kappa = 1/2, 1, 2, 4$, respectively. The horizon has been set to $v_H = 0$ for all the motions. The mirror starts asymptotically static, but has uniform acceleration in the far future.

The trajectory in spacetime coordinates is plotted in a spacetime plot Fig. 3. A conformal diagram of the accelerated boundary is given in Fig. 4.

The rapidity, η, as defined through [22],

$$f'(v) = e^{-2\eta(v)} \to \eta(v) = -\frac{1}{2}\ln\frac{df(v)}{dv}, \tag{8}$$

as a function of advanced time, is

$$\eta(v) = \ln\left(1 - \frac{1}{\kappa(v_H - v) + 1}\right). \tag{9}$$

The limit in the far past, $v \to -\infty$ is $\eta \to 0$; the mirror is past asymptotically "static." That is, only in the sense that velocity approaches zero; but technically, the Minkowski spatial coordinate, $x = \frac{1}{2}(v - u)$ diverges in the far past, $x \to +\infty$, as $v \to -\infty$. The early time behavior of the trajectory underscores the nonuniform acceleration and striking difference in past vs future states. The future limit as advanced time $v \to v_H$, from below, is $\eta \to -\infty$. The mirror rapidly travels left, off to the speed of light. The proper acceleration [22], through

$$\alpha(v) = e^{\eta(v)}\frac{d\eta(v)}{dv}, \tag{10}$$

is a notably simple monotonic function of v,

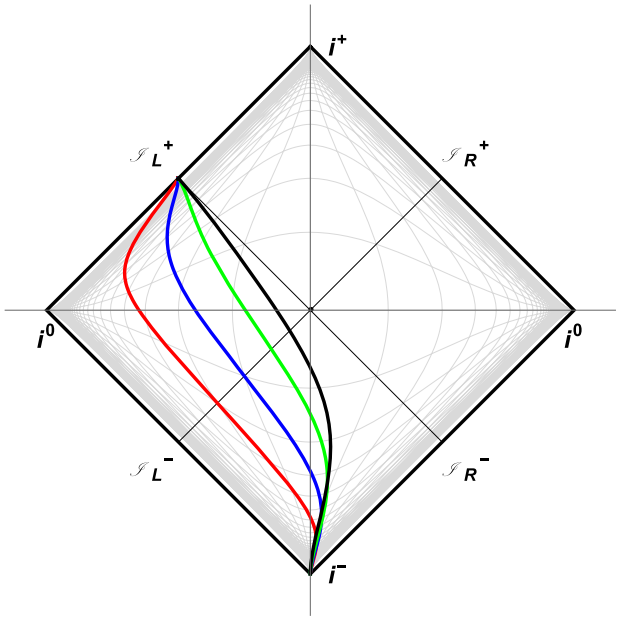

FIG. 4. The trajectory Eq. (7), in a Penrose conformal diagram, with different scaling for asymptotic future proper acceleration, κ. The red, blue, green, black curves correspond to $\kappa = 1/2, 1, 2, 4$, respectively. This is the same color scheme of Fig. 3. The horizon has been set to $v_H = 0$ for all the motions.

$$\alpha(v) = -\frac{\kappa}{(\kappa(v_H - v) + 1)^2}. \tag{11}$$

In the limit that advanced time approaches the horizon,

$$\lim_{v \to v_H} \alpha = -\kappa. \tag{12}$$

This character is the key defining dynamic trait of the mirror, i.e., the mirror becomes uniformly accelerating in the far future. Both the magnitudes of rapidity and acceleration are plotted in Fig. 5 as a function of advanced time, $-\infty < v < v_H = 0$.

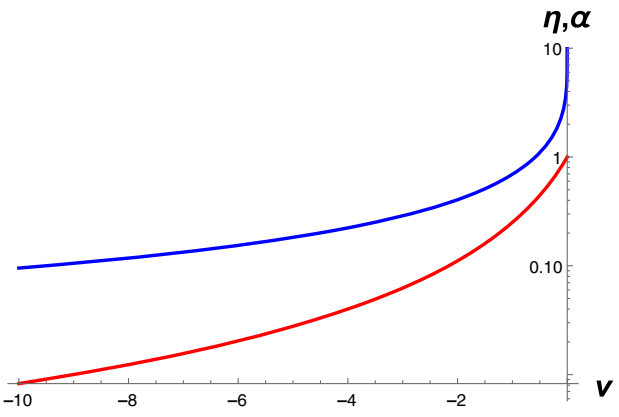

FIG. 5. The rapidity, $|\eta(v)|$ of Eq. (9), is illustrated in a log plot by the blue line that diverges (the mirror approaches the speed of light) at the $v_H = 0$ horizon, where $\kappa = 1$ units. The proper acceleration, $|\alpha(v)|$, of Eq. (11), is illustrated in red, and asymptotically approaches κ which has been set to $\kappa = 1$.

IV. STRESS TENSOR AND TOTAL ENERGY

A. Stress tensor

Balbinot *et al.* [23] found that the stress energy tensor of the nonextremal RN black hole stays regular in the extremal limit and smoothly transitions to that of nonextreme black holes. Contrary to previous studies, it was shown that the expectation values of the quantum stress energy tensor for our massless scalar field living on a $1+1$ dimensional ERN black hole background are indeed completely regular on the horizon [20]. These results provide confidence to utilize the stress tensor in the moving mirror model, integrated to the horizon, which we use to find total evaporation energy. The moving mirror stress-energy tensor resulting from point splitting [6,7,22] in light cone coordinates is $\langle T_{uv} \rangle = \langle T_{vu} \rangle = \langle T_{vv} \rangle = 0$, with the only nonzero component being the Schwarzian derivative of Eq. (6) [24],

$$\langle T_{uu} \rangle := F(v) = \frac{1}{24\pi}\{f(v), v\} f'(v)^{-2}, \tag{13}$$

where the Schwarzian brackets are defined as

$$\{f(v), v\} \equiv \frac{f'''}{f'} - \frac{3}{2}\left(\frac{f''}{f'}\right)^2, \tag{14}$$

which yields

$$F(v) = \frac{\kappa^2}{6\pi} \frac{(\kappa(v_H - v))^3}{(\kappa(v_H - v) + 1)^6}. \tag{15}$$

The maximum flux, $F_m = (384\pi M^2)^{-1}$, is half as much as the usual Hawking flux for a Schwarzschild black hole, $F_H = (768\pi M^2)^{-1}$, comparing equal mass stars ("charged" vs uncharged). Even though charged black holes are colder than neutral black holes, recall that the ERN cannot be characterized by temperature [1,2], so it is not actually cooler, in spite of the intuitive result, $F_H = 2F_m$.

It is worth mentioning there is no transient negative energy flux. Recall that advanced time ranges from $-\infty < v \leq v_H$. This range is illustrated in Fig. 6, and one observes the flux is always positive. This is a relatively unusual trait among solved moving mirrors, as all currently (2020) solved drifting mirrors are accompanied by negative energy flux (e.g., [25]). Negative energy flux is a requirement for mirrors that are asymptotically static or drifting [26]. To look across space, we can express the flux in spacetime coordinates via

$$F(x) = \frac{1}{12\pi} \frac{t'''(t'^2 - 1) - 3t't''^2}{(t' - 1)^4 (t' + 1)^2}, \tag{16}$$

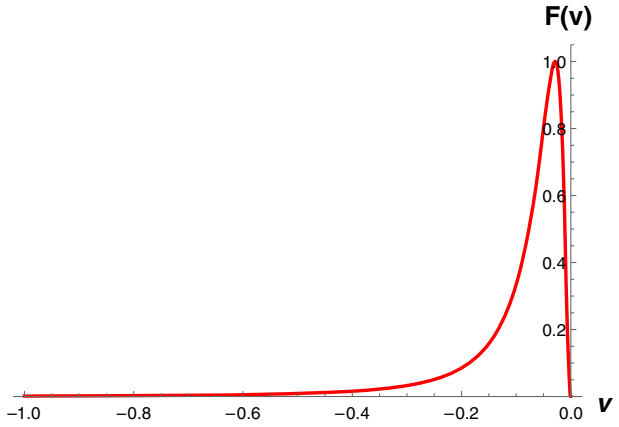

FIG. 6. The energy flux, $F(v)$, Eq. (15), radiated by the ERN moving mirror is illustrated in advanced time with horizon at $v = v_H = 0$. The units are $\kappa = \sqrt{384\pi}$, so that the maximum flux is normalized to $F_m = 1$. The time is $v = -1/\kappa = -2M$, when the flux is maximum.

where primes are derivatives with respect to space coordinate x. One gets

$$F(x) = \frac{4\kappa^2}{3\pi}\frac{W(\frac{1}{2}e^{-\kappa x})^3}{(2W(\frac{1}{2}e^{-\kappa x})+1)^6}. \tag{17}$$

This form is more intuitive, since there is no bound in space, i.e., the mirror covers the space, $+\infty > x > -\infty$, i.e., it travels the entire Minkowski grid, but starting from $x = +\infty$, moving left. The flux, $F(x)$, is plotted in Fig. 7.

B. Total energy

The total energy observed by our observer at $\mathcal{I}_R^+$ (see e.g., [27]) is worth calculating, even though the mirror accelerates forever, using Eqs. (15) and (6),

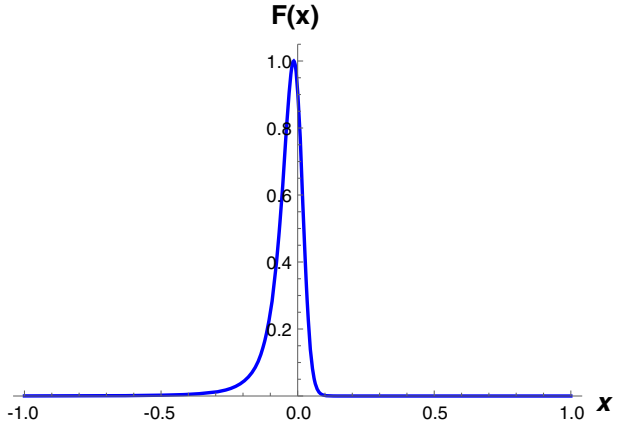

FIG. 7. The energy flux, Eq. (17), radiated by the ERN moving mirror is illustrated in space, $F(x)$, by the blue line, in units where $\kappa = \sqrt{384\pi}$, so that the maximum flux is normalized to $F_m = 1$. The location this happens at is $x = -1/(2\kappa) = -M$. Recall that the mirror moves to the left, so that $x = +\infty$ is asymptotic past times, $t = -\infty$. By plotting in space, x, we have extended the coordinate variable to all ∞, in contrast to Fig. 6.

$$E = \int_{-\infty}^{v_H} F(v)\frac{df(v)}{dv}dv, \tag{18}$$

where we integrate over delayed time, du, necessitating the introduction of the Jacobian $f'(v)$, and only up to the horizon, v_H. The spacetime result, Eqs. (17) and (7), is also convenient via numerical integration,

$$E = \int_{+\infty}^{-\infty} F(x)\left(\frac{dt(x)}{dx} - 1\right)dx, \tag{19}$$

because the bounds are infinite, remembering the mirror moves to the left starting at $x = +\infty$. The total energy result is analytic,

$$E = \frac{\hbar\kappa}{36\pi}. \tag{20}$$

While positive flux is accordant, finite energy is more than welcome. All known asymptotically drifting mirrors emit a finite amount of energy (see e.g., [28–30]). In contrast, most known null mirrors, i.e., those that attain the speed of light, produce an infinite amount of energy. This mirror maintains finite nonzero energy and asymptotic light speed with its eternal asymptotic constant acceleration.[3] The finite energy, E, of Eq. (20), prevents the formation of a naked singularity by the emission of neutral scalar particles, since the evaporation of the energy carrying particles is strictly limited.

V. SPECTRUM AND PARTICLE COUNT

As we have mentioned, LRS [1] are well aware that the quantum radiation emitted by an incipient extremal black hole is not characterized by a temperature at any time during collapse, which has been backed up by Anderson-Hiscock-Taylor who found that macroscopic *zero temperature* black hole solutions do not exist [2]. The radiation is not characterized by temperature or a Planck distribution at all. Our results confirm these findings, and we extend this program of investigation further by solving for and analyzing the nonthermal spectrum. The beta Bogolubov coefficient can be found via

$$\beta_{\omega\omega'} = \frac{-1}{4\pi\sqrt{\omega\omega'}}\int_{-\infty}^{v_H} dv e^{-i\omega' v - i\omega f(v)}(\omega f'(v) - \omega'), \tag{21}$$

by setting the horizon $v_H = 0$ for convenience and definiteness (horizon position will not affect the spectrum because of complex conjugation). The result is

[3]One unsolved mirror that has finite energy but accelerates to infinite proper acceleration is investigated in [31].

$$\beta_{\omega\omega'} = \frac{-ie^{-\frac{\pi\omega}{\kappa}}}{\pi\kappa}\sqrt{\frac{\omega'}{\omega_p}}\left(\frac{\omega}{\omega_p}\right)^{\frac{i\omega}{\kappa}} K_a\left(\frac{2}{\kappa}\sqrt{\omega\omega_p}\right), \quad (22)$$

where $\omega_p \equiv \omega + \omega'$, and $a \equiv \frac{2i\omega}{\kappa} + 1$. On our way to obtain the spectrum, the complex conjugate is taken,

$$|\beta_{\omega\omega'}|^2 = \frac{e^{-\frac{2\pi\omega}{\kappa}}\omega'}{\pi^2\kappa^2\omega_p}\left|K_a\left(\frac{2}{\kappa}\sqrt{\omega\omega_p}\right)\right|^2, \quad (23)$$

which is the particle count per mode squared. The spectrum, which is the main result of this paper, along with its time localization Eq. (28), is then

$$N_\omega = \int_0^\infty |\beta_{\omega\omega'}|^2 d\omega', \quad (24)$$

plotted in Fig. 8. An infrared divergence, signaling soft particles [32], and infinite total particle count,

$$N = \int_0^\infty |\beta_{\omega\omega'}|^2 d\omega d\omega', \quad (25)$$

is illustrated. The divergence of global particle count at zero frequency is unsolved in the moving mirror model for nonasymptotically static mirrors [33,34]. At this juncture, it is good to test our intuition, that the particles (even though infinite) carry the energy [35]. A consistency check is warranted on the result, Eq. (23). Summing up all the energies of each particle should yield the total finite energy:

$$E = \int_0^\infty \omega|\beta_{\omega\omega'}|^2 d\omega d\omega' = \frac{\hbar\kappa}{36\pi}. \quad (26)$$

Indeed, this is not hard to check. The result confirms the answer, Eq. (20), obtained by use of the stress tensor.

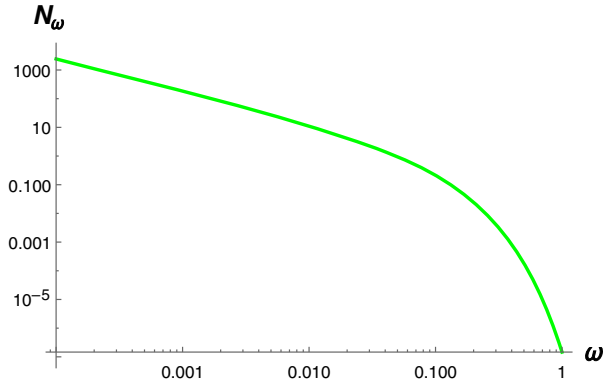

FIG. 8. The particle spectrum, Eq. (24), in a log-log plot, demonstrating an infrared divergence, for $\omega \to 0$. This signals infinite total particle count due to the soft particles at $\omega = 0$.

A. Time evolution of particle production

The time dependence of particle creation can be computed via wave packet analysis suggested by Hawking [9], and elaborated by others [26,36]. Wave packet localization, particularly via orthonormal and complete sets in the moving mirror model is described in detail in several works [25,37–39]. A plot of the particle creation in time is given in Fig. 9. The rate of emission of particles is finite in a given time and frequency interval which can be seen by constructing a complete orthonormal family of wave packets from the beta Bogolubov coefficients. Following Hawking's notation, we let

$$\beta_{jn\omega'} = \frac{1}{\sqrt{\epsilon}}\int_{j\epsilon}^{(j+1)\epsilon} d\omega e^{2\pi i\omega n/\epsilon}\beta_{\omega\omega'}, \quad (27)$$

where $j \geq 0$ and n are integers. These packets are built at future right null infinity, $\mathcal{I}_R^+$, and peak at delayed exterior time, $u = 2\pi n/\epsilon$, with width $2\pi/\epsilon$. Therefore the vertical axis in Fig. 9 has a discrete and intuitive physical interpretation, giving the counts of a particle detector sensitive only to frequencies within ϵ of $\omega_j = j\epsilon$, for a time $2\pi/\epsilon$ at $u = 2\pi n/\epsilon$. Late times correspond to large quantum number n. For excellent time resolution, only one frequency bin is needed, where the particles pile up, $j = 0$, and a relatively large value of ϵ resolves the count in time. Following the text of Fabbri-Navarro-Salas [19], Fig. 9 may be reconstructed by first packetizing the beta coefficient as done in Eq. (27), second numerically integrating over ω' from 0 to ∞ as in Eq. (24), and third, computing the results, N_{jn},

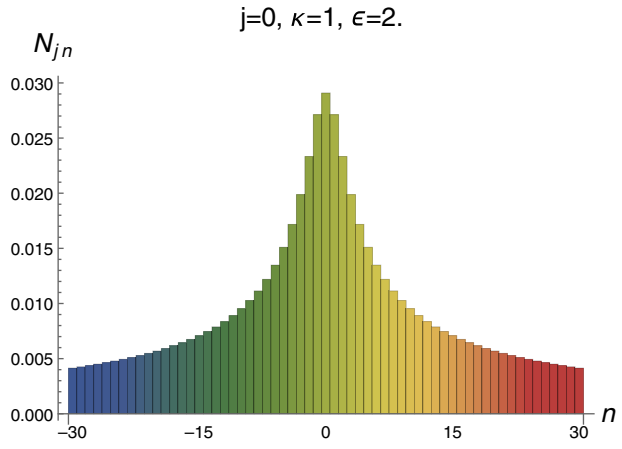

FIG. 9. The particle count in time, via wave packet localization. The detector is set with $\epsilon = 2$. The scale of the system is $\kappa = 1$ and the frequency bin is in the lowest possible $j = 0$ value, where most of the particle production occurs, and finer resolution in time is possible. This emission includes the "phantom radiation" of [1]. It is symmetric in delayed time, u, centered around time bin $n = 0$.

$$N_{jn} = \int_0^{+\infty} d\omega' |\beta_{jn\omega'}|^2, \tag{28}$$

for each individual time bin, n, for a set frequency bin, j (in our fine-grained time resolution case, $j = 0$).

The symmetric distribution of particle production in Fig. 9 looks at odds with the asymmetric energy flux production of $F(x)$ and $F(v)$ in Figs. 6 and 7, respectively. The energy is carried by the particles, as we have seen, but is it carried asymmetrically in time? The time bins n correspond to delayed time $u = t - x$. This compels a third look at the flux, now as $F(u)$, to confirm suspicion that the asymmetry is a coordinate artifact. This can be done numerically, by an inverse function technique applied to $f(v)$, Eq. (6). Using asymptotic acceleration units, the result for the flux is

$$F(u) = -\frac{p(u)^3}{6\pi(p(u)-1)^6}, \tag{29}$$

plotted in Fig. 10. The result is symmetric in delayed time u, and the total integrated flux,

$$E = \int_{-\infty}^{+\infty} F(u) du, \tag{30}$$

is in agreement with the total energy, Eq. (20). The symmetry here confirms the energy is carried symmetrically in delayed time, u, as also observed by a detector at $\mathcal{I}_R^+$, receiving the particles, delayed in time, u.

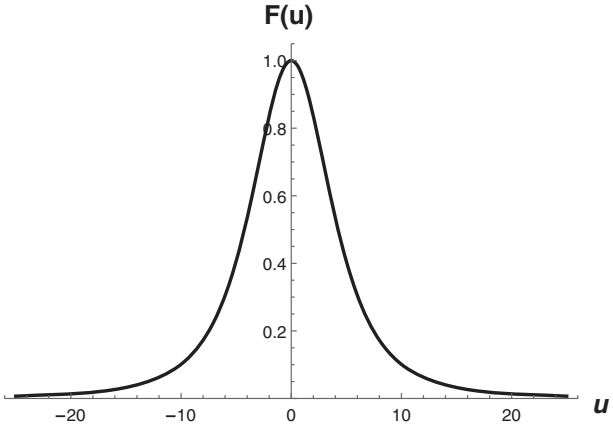

FIG. 10. The energy flux, $F(u)$, Eq. (29), radiated by the ERN moving mirror is illustrated in delayed time u with horizon at $v = v_H = 0$. The units are $\kappa = \sqrt{384\pi}$, so that the maximum flux is normalized to $F_m = 1$. The time is $u = 0$, when the flux is maximum. This plot demonstrates symmetry in delayed time, reflecting the symmetry of particle production in delayed time bins, n, of Fig. 9.

B. Uniform acceleration spectra

To ensure consistency of the results at late times, it is necessary to compare the spectra of uniform acceleration with the ERN spectra, Eq. (23). The uniformly accelerated mirror, $\alpha = -\kappa$,

$$p(u) = \frac{u}{1+\kappa u}, \tag{31}$$

with early-time horizon positioned at $u_H = -\kappa^{-1}$, has a spectrum that is solved via

$$\beta_{\omega\omega'} = \frac{1}{4\pi\sqrt{\omega\omega'}} \int_{-\kappa^{-1}}^{\infty} du e^{-iu\omega - i\omega' p(u)} (\omega' p'(u) - \omega), \tag{32}$$

via a simple substitution, $1 + \kappa u = \kappa X$, so that the range of integration can be extended over X. A Heaviside theta function assists in further extension to cover $(-\infty, +\infty)$ integration. The result is

$$\beta_{\omega\omega'} = \frac{i e^{\frac{i(\omega-\omega')}{\kappa}}}{\pi\kappa} K_1\left(\frac{2}{\kappa}\sqrt{\omega\omega'}\right). \tag{33}$$

The phase vanishes upon complex conjugation,

$$|\beta_{\omega\omega'}|^2 = \frac{1}{\pi^2\kappa^2} \left| K_1\left(\frac{2}{\kappa}\sqrt{\omega\omega'}\right)\right|^2. \tag{34}$$

This is the spectrum of a uniformly accelerated mirror, distinctly nonthermal [7,8,14]. It is straightforward to compare Eq. (34) with Eq. (23) at late times to leading order, using the high frequency limit [9], $\omega' \gg \omega$, and one finds identical spectra. The qualitative idea connecting late times to this high frequency limit is that in the far future incoming modes that reflect off the mirror become extremely redshifted by the very fast (near the speed of light) receding boundary. The main contribution to the beta coefficient comes from very high frequency incoming modes, and therefore are governed by the asymptotic form, Eq. (34), for high $\omega' \gg \omega$ which is independent of the details of the collapse.

VI. DISCUSSION

The connection between the moving mirror in flat spacetime and the collapsing star in curved space is most closely characterized by the matching condition, Eq. (5), and the moving mirror position, Eq. (6). The matching condition is the delayed outside light coordinate position, $u(U)$, of the origin of the incipient black hole expressed as a function of the delayed inside light coordinate, U. In the moving mirror case, this is the delayed light coordinate position, $f(v)$, of the boundary as a function of the advanced light coordinate position, v. It is the regularity condition on the field modes that allows the curved spacetime system to be described in the more simple

setting of flat spacetime by an accelerated perfectly reflecting boundary. The fact that the origin effectively reflects the modes, where no field exists behind $r < 0$, assists in the exact calculation of the resulting particle creation from the beta Bogolubov coefficients, Eq. (22). In the following two subsections we address some immediate and interesting limitations and extensions of this connection.

A. Limitations

Our approach has been to keep everything as simple as possible by utilizing the moving mirror model, but the need to accept complications when clearly unavoidable is obviously present with respect to numerous physical aspects. While conceptually clear, the extremal RN moving mirror model is ultimately extremely limited, for instance:

(i) Gray-body factors: The spectra will be altered by backscattering [1,19] and the nontrivial metric coefficients of spacetime. These affects are not accounted for in the moving mirror model.

(ii) Dimensionality and spherical symmetry: In order to appropriately generalize to $3+1$ dimensions, the powerful simplification due to spherical symmetry apparently severally restricts utilization of the model; however some aspects have carry-over [40], e.g., zero surface gravity.

An additional important caveat here is the nature of the fine-tuned collapse. LRS assumed that models can be found in which collapse leads to a black hole with maximum charge [1]. The fine-tuning required to produce extremal solutions makes the question of their existence nontrivial [41]. The fine-tuning exists because of the extreme sensitivity to effects of backreaction [42] of the quantum radiation on the metric or the mirror. Nevertheless, as we have shown, interesting information can be found by assuming collapse occurs and deducing the consequences.

B. Extensions

Immediate extensions are possible. First, a calculation of the variance of the stress tensor is warrented. The asymptotic value of the two-point function does not tend to zero which is the thermal emission value. This could shed light on the information contained in the stress energy above and beyond what is apparent from the tensor alone, i.e., exponential fast damping exhibited by nonextreme collapse vs power law damping exhibited by the ERN solution [1].

Second, and particularly interesting, is a better understanding of the $\omega = 0$ singularity responsible for the soft particle divergence [32]. Removal by radiative corrections analogous to bremsstrahlung cross section cancellation may be possible [1], accounting for momentum transfer from field to mirror (recoil). It may also be possible to simply regularize the spectrum by the uniform acceleration contribution, since only soft particles are characterized by these colors.

Third, a concrete demonstration of the (in)stability [41,43,44] of the moving mirror dynamics would be useful, as early collapse emission could cause asymptotic runaway acceleration or asymptotic zero acceleration, pushing the system out of gravitational-electrical equilibrium. Different dynamics can lead to a calculation of radiation for the nonextreme RN mirror. We will demonstrate this spectrum in a separate paper.

VII. CONCLUSIONS

We have solved the ERN black hole–moving mirror correspondence.[4] In particular we have made progress on several fronts:

(i) Trajectory: We have identified a flat spacetime moving mirror trajectory that models the collapse of a null shell to an ERN black hole. The acceleration is not uniform: it increases from zero at asymptotically early times to a nonvanishing constant at asymptotically late times. Measurement of particle production at early times can violate the no-hair theorem, demonstrating details specific to the form of collapse.

(ii) Finite energy: Despite reaching asymptotic light speed, with never ending uniform acceleration, the evaporation process finishes. This is signaled by the computed finite energy, $E = (72\pi M)^{-1}$.

(iii) Spectra: We have derived the analytic global (time-nonlocalized) beta coefficients for evaluation of the spectra. Detection, even if possible, of arbitrarily low frequency soft particles at late times registering nonzero detector probability, will not allow one to determine the spectra of collapse. Having the time-nonlocalized spectra, in the form $|\beta_{\omega\omega'}|^2$, means we can possibly screen our detector from the noninformative (no information-carrying) flux of soft particles.

(iv) Time evolved particle count: The evolution (time localized) of particle creation is demonstrably nonthermal, and in fact peaks in out-of-equilibrium early time. The nonsteady rate explicitly verifies a non-Planckian distribution. The particle count is damped in the far past and far future. The ERN black hole releases information (e.g., [49]) quickly (before late times) and the half-way point of collapse is reminiscent of [50] where the black hole acts like a quantum information mirror.

With respect to (1) the cosmic censorship conjecture (CCC) and (2) the no-hair theorem: (1) we have shown that quantized fields can preserve the CCC, preventing the formation of a naked singularity analog in the mirror

[4]The Schwarzschild mirror is solved here: [45–48].

system, by demonstrating the limiting energy emission and late-time zero energy flux. The ERN does not lose mass at late times. Thus, we maintain cosmic censorship. (2) The no-hair theorem is seemingly violated because the particle spectrum (as computed from the global beta coefficients), valid for nonlocalized and localized times, is dependent on the evolution of initial collapse. The key difference is the late-time behavior, which in fact does not depend on the details of early collapse, actually preserves the late-time no-hair theorem. You lose hair when you are old.

ACKNOWLEDGMENTS

M. G. thanks Paul Anderson, Eric Linder, Yen Chin Ong, and Daniele Malafarina for stimulating discussions. Funding from state-targeted program "Center of Excellence for Fundamental and Applied Physics" (BR05236454) by the Ministry of Education and Science of the Republic of Kazakhstan is acknowledged. M. G. is also funded by the FY2018-SGP-1-STMM Faculty Development Competitive Research Grant No. 090118FD5350 at Nazarbayev University.

[1] S. Liberati, T. Rothman, and S. Sonego, Phys. Rev. D **62**, 024005 (2000).
[2] P. R. Anderson, W. A. Hiscock, and B. E. Taylor, Phys. Rev. Lett. **85**, 2438 (2000).
[3] A. Strominger and C. Vafa, Phys. Lett. B **379**, 99 (1996).
[4] V. V. Dodonov, MDPI Phys. **2**, 67 (2020).
[5] G. T. Moore, J. Math. Phys. (N.Y.) **11**, 2679 (1970).
[6] B. S. DeWitt, Phys. Rep. **19**, 295 (1975).
[7] S. A. Fulling and P. C. W. Davies, Proc. R. Soc. A **348**, 393 (1976).
[8] P. C. W. Davies and S. A. Fulling, Proc. R. Soc. A **356**, 237 (1977).
[9] S. W. Hawking, Commun. Math. Phys. **43**, 199 (1975).
[10] A. A. Svidzinsky, J. S. Ben-Benjamin, S. A. Fulling, and D. N. Page, Phys. Rev. Lett. **121**, 071301 (2018).
[11] M. R. R. Good and E. V. Linder, arXiv:2003.01333.
[12] W. G. Unruh, Phys. Rev. D **14**, 870 (1976).
[13] S. Liberati, T. Rothman, and S. Sonego, Int. J. Mod. Phys. D **10**, 33 (2001).
[14] N. D. Birrell and P. C. W. Davies, *Quantum Fields in Curved Space* (Cambridge University Press, Cambridge, England, 1982).
[15] R. D. Carlitz and R. S. Willey, Phys. Rev. D **36**, 2327 (1987).
[16] M. R. R. Good, Int. J. Mod. Phys. A **28**, 1350008 (2013).
[17] W. A. Hiscock, Phys. Rev. D **23**, 2813 (1981).
[18] B. Carter, Phys. Lett. **21**, 423 (1966).
[19] A. Fabbri and J. Navarro-Salas, *Modeling Black Hole Evaporation* (Imperial College Press, London, 2005).
[20] R. Balbinot, S. Fagnocchi, A. Fabbri, S. Farese, and J. Navarro-Salas, Phys. Rev. D **70**, 064031 (2004).
[21] F. Wilczek, *International Symposium on Black holes, Membranes, Wormholes and Superstrings* (1992), pp. 1–21 [arXiv:hep-th/9302096].
[22] M. R. R. Good and E. V. Linder, Phys. Rev. D **97**, 065006 (2018).
[23] R. Balbinot, A. Fabbri, S. Farese, and R. Parentani, Phys. Rev. D **76**, 124010 (2007).
[24] M. R. R. Good, K. Yelshibekov, and Y. C. Ong, J. High Energy Phys. 03 (2017) 013.
[25] M. R. R. Good, *Kerson Huang Memorial* (World Scientific, Singapore, 2017), pp. 113–116, https://doi.org/10.1142/9789813207431_0014.
[26] M. R. R. Good, E. V. Linder, and F. Wilczek, Phys. Rev. D **101**, 025012 (2020).
[27] V. I. Ritus, J. Exp. Theor. Phys. **83**, 282 (1996).
[28] M. R. R. Good, Y. C. Ong, A. Myrzakul, and K. Yelshibekov, Gen. Relativ. Gravit. **51**, 92 (2019).
[29] M. R. R. Good, Universe **4**, 122 (2018).
[30] A. Myrzakul and M. R. R. Good, *15th Marcel Grossmann Meeting on Recent Developments in Theoretical and Experimental General Relativity, Astrophysics, and Relativistic Field Theories* (2018) [arXiv:1807.10627].
[31] M. R. R. Good and E. V. Linder, Phys. Rev. D **99**, 025009 (2019).
[32] S. W. Hawking, M. J. Perry, and A. Strominger, Phys. Rev. Lett. **116**, 231301 (2016).
[33] W. R. Walker and P. C. W. Davies, J. Phys. A **15**, L477 (1982).
[34] M. R. R. Good and E. V. Linder, Phys. Rev. D **96**, 125010 (2017).
[35] W. R. Walker, Phys. Rev. D **31**, 767 (1985).
[36] M. R. R. Good, E. V. Linder, and F. Wilczek, Mod. Phys. Lett. A **35**, 2040006 (2020).
[37] M. R. R. Good, P. R. Anderson, and C. R. Evans, Phys. Rev. D **88**, 025023 (2013).
[38] E. Martin-Martinez, M. Montero, and M. del Rey, Phys. Rev. D **87**, 064038 (2013).
[39] M. R. R. Good and Y. C. Ong, J. High Energy Phys. 07 (2015) 145.
[40] T. Rothman, Phys. Lett. A **273**, 303 (2000).
[41] P. Anninos and T. Rothman, Phys. Rev. D **65**, 024003 (2001).
[42] D. Marolf, Gen. Relativ. Gravit. **42**, 2337 (2010).
[43] P. R. Anderson, W. A. Hiscock, and D. J. Loranz, Phys. Rev. Lett. **74**, 4365 (1995).
[44] S. Hod, Phys. Lett. B **713**, 505 (2012).
[45] M. R. R. Good, P. R. Anderson, and C. R. Evans, Phys. Rev. D **94**, 065010 (2016).
[46] M. R. R. Good, *2nd LeCosPA Symposium: Everything about Gravity, Celebrating the Centenary of Einstein's General Relativity* (2017), pp. 560–565, https://doi.org/10.1142/9789813203952_0078.

[47] P. R. Anderson, M. R. R. Good, and C. R. Evans, *14th Marcel Grossmann Meeting on Recent Developments in Theoretical and Experimental General Relativity, Astrophysics, and Relativistic Field Theories* (2017), pp. 1705–1708, https://doi.org/10.1142/9789813226609_0172.

[48] M. R. R. Good, P. R. Anderson, and C. R. Evans, *14th Marcel Grossmann Meeting on Recent Developments in Theoretical and Experimental General Relativity, Astrophysics, and Relativistic Field Theories* (2017), pp. 1701–1704, https://doi.org/10.1142/9789813226609_0171.

[49] J. D. Bekenstein and A. E. Mayo, Gen. Relativ. Gravit. **33**, 2095 (2001).

[50] P. Hayden and J. Preskill, J. High Energy Phys. 09 (2007) 120.